PCCP

ROYAL SOCIETY OF CHEMISTRY

COMMUNICATION

View Article Online
View Journal | View Issue



Cite this: *Phys. Chem. Chem. Phys.*, 2020, **22**, 10828

Received 25th March 2020,
Accepted 27th April 2020

DOI: 10.1039/d0cp01621g

rsc.li/pccp



# Introducing mesoscopic charge transfer rates into molecular electronics†

Adriano Santos, [a] Ushula M. Tefashe, [b] Richard L. McCreery *[b] and Paulo R. Bueno *[a]

**It has been demonstrated that mesoscopic rates operate in nanoscale electrochemical systems and, from a fundamental point of view, are able to establish a bridge between electrochemical and molecular electronic concepts. In the present work we offer additional experimental evidence in support of this statement.**

Mesoscopic terminology refers to systems with properties and energetic states between classical and quantum mechanical limits.[1] The purpose of this communication is to demonstrate that the analysis of mesoscopic rates can describe both heterogeneous electron transfer reactions and transport in molecular electronic devices, thus harmonizing the physical principles of electrochemistry with those of molecular electronics. Hence, in this communication, we introduce the potential applications of mesoscopic rates and related concepts of quantum conductance and capacitance into molecular electronics, demonstrating that the chemical capacitance $C_\mu$ is an important missing parameter for the correlation between both heterogeneous electron transfer reactions and transport in molecular electronic devices. In addition, frequency dependent phenomena revealed by impedance spectroscopy (IS) data provide insights about molecular junctions (MJs) not available from standard current–voltage ($I$–$V$) measurements.

As it is well-known, electron transport phenomena in molecules are of scientific interest[2–10] but also have applications in commercial devices.[1,11] Electron transport governs commercial devices which represent a significant portion of tech industry. For instance, we can refer to transistors as distinctive electronic components of the semiconductor industry which are essential in fabricating chips and computers where electron transport is crucial. Our ability to fabricate electron conducting channels in transistors on a nanoscale is a limiting factor on achievable computer power. Furthermore, the architecture of these channels determines the applications of electronic devices. An important example is when operating in sensors, these channels are sensitive to changes in their environments – as in the case of field-effect transistors. The smaller the size of conducting channels in transistors, the more computer power we are able to squeeze into chips, but the physics governing channels with widths less than ~8 nm involves mesoscopic concepts distinct from those of classical semiconductors.

Heterogeneous electron transport governed mainly by activated Marcus and Butler–Volmer kinetics is of obvious importance to the operation of electrochemical devices,[1,11–14] including the ubiquitous batteries found in portable consumer electronics. As described above, we can split the movement of electrons into electron transport (electronics) and electron transfer (electrochemistry),[1,11,15,16] but this is, to some extent, a false dichotomy which is reinforced by nomenclature. A comparison between electronics and electrochemistry from the perspective of mesoscopic physics demonstrates that these fields are fundamentally interrelated.[1,2,11,17,18]

The relationship between these two apparently distinct scientific areas is embodied by an electron transfer rate which occurs in a defined length scale and is fundamental at any molecular or mesoscopic scale.[1,11] Herein we will refer to this rate simply as $k$, with a unit of $s^{-1}$. Note that the effect of solvent reorganization energy can be considered in the model of $k$, as introduced here, whenever it is appropriate,[16] but this is more particularly important in the context of molecular junctions. To explain the meaning of $k$ in the context of electrochemistry and molecular electronics let us consider two types of configurations, where electron injection rates are observed in both electrochemistry and molecular electronic configurations of measurements, as depicted in Fig. 1. Several mechanisms have been considered for explaining electron transport in molecular junctions, including tunneling,[19–21] Marcus-like activated transfer,[22,23] injection[24,25] and resonant transport.[26–28] Since these phenomena have analogs in electrochemical redox reactions on modified electrodes with different boundary conditions, we consider here how well the

[a] *Institute of Chemistry, São Paulo State University (UNESP), 55 Prof. Francisco Degni St., Araraquara, São Paulo, 14800-060, Brazil. E-mail: paulo-roberto.bueno@unesp.br*

[b] *Department of Chemistry, University of Alberta, Edmonton, Alberta T6G 2G2, Canada. E-mail: richard.mccreery@ualberta.ca*

† Electronic supplementary information (ESI) available: Results of data fitting of raw EIS data using equivalent circuit and $C_\mu$ in function of bias potential. See DOI: 10.1039/d0cp01621g

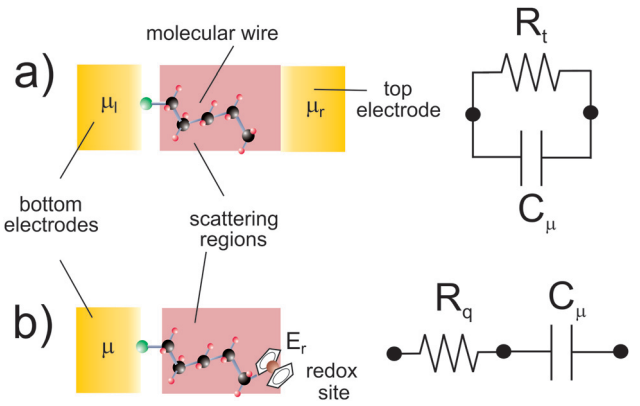


Fig. 1 (a) Typical configuration used to study molecular conductance in an electrochemical setup where injections are made from the electrode to the redox centers intermediated by a molecular bridge. (b) Configurations used in molecular electronics. Other terms of the circuit such as contact resistance ($R_c$), *etc.* were omitted for the sake of simplicity and to focus on the meaning of $k$.

mesoscopic treatment applies to both molecular electronics and electrochemical charge transfer.

In Fig. 1(a) we illustrate a common electrochemical configuration where redox tagged self-assembled molecules are attached to a metallic electrode and where the electron injections are made from the electrode into the redox states through a molecular "wire" which contacts the electrode and redox states.[1,11] Using mesoscopic terminology, the redox center is considered a capacitor, $C_{\bar{\mu}}$, with distinct properties compared to a conventional parallel-plate capacitor. In this case, the rate of electron transport is $k = G/C_{\bar{\mu}}$, where $C_{\bar{\mu}}$, is the electrochemical capacitance and $G = 1/R$ is the quantum of conductance. $C_\mu$ in Fig. 1(b) includes the capacitance as result of charge injection into molecular orbitals, and this is chemically comparable to a redox event at the molecular level. Both $C_{\bar{\mu}}$ and $C_\mu$ in Fig. 1 can be modelled as capacitors, but in the electrochemical case there are additional effects associated with mobile ions and electrode screening. As will be discussed below, both electrochemistry and molecular conductance in solid-state devices involve electron transfer with a characteristic rate, though ions, solvent, and electrode screening are modifications applicable primarily to electrochemistry.

The fact that the $k = G/C_\mu$ relationship[1,11] can be restated as $G = kC_\mu$ establishes that electron transport is dependent on $C_\mu$ regardless of the configuration (electrochemistry or electronics) used to measure the molecular conductance.[29] The debate between the equivalence of conductance inferred from molecular electronics and from electrochemistry has been actively discussed over the last decade.[2,18,29,30] We demonstrated in previous reports,[1,11] that the meaning of $k$ is able to reconcile the debate.[29,30] It is important to note that $k$ is proportional to $1/C_\mu$ which is a series combination ($1/C_\mu = 1/C_e + 1/C_q$) of electrostatic $C_e$ and quantum $C_q$ capacitances.[1,11] $C_e$ is only dependent on dielectric properties and geometric factors and $C_q$ accounts for the contributions of the molecular orbitals and redox states to $k$.

The simple relationship between rate, quantum conductance and electrochemical capacitance demonstrates that electronics and electrochemistry are conceptually equivalent, at least at the molecular scale, where the $G = kC_\mu$ relationship has been proved to be valid and where both $G$ and $C_\mu$ can be deduced from first-principle quantum mechanics.[1,11] Furthermore, $k$ has already been demonstrated to be useful for describing different practical situations in electrochemistry.[1,11,16] For instance, it has been used to access the energy for charging molecular redox switches,[1,11] in quantifying the discharge of these switches as the operative transducer signal in biosensors,[31] in obtaining the conductance of DNA functioning as molecular wires,[32] in explaining the pseudocapacitance in $TiO_2$ nanotubes[33] and finally in explaining the super-capacitance of reduced graphene[34] and so on.

It is important to note that for a given energy $E$ (= $eV$), $G$ is defined as $G(E) = G_0 \sum_n T_n(E)$, where $G_0 = 2e^2/h$ is a constant and $\sum_n T_n(E)$ is the transmission probability over a given number of channels, $n$. Note that through $\sum_n T_n(E)$ transmission coefficients can be determined. For instance, assuming a $T(E,L)$ which is a function of $E$ and the length $L$, a $T(E,L) \propto e^{-\beta L}$ can be defined in cases of tunneling through a large barrier.

Turning to the impedance analysis of MJs (details of MJs preparation is in ESI,† ESI-1), the points in Fig. 2 show Nyquist impedance spectra‡ for Au/eC/azobenzene/eC/Au junctions (eC = electron beam deposited carbon)[35] of seven different molecular layer thicknesses, which demonstrates the strong dependence of $R = 1/G$ on thickness. The lines in Fig. 2 are fits of the experimental results to the equivalent circuit model as shown in Fig. 1(b), from which $k$, $G$ and $C_\mu$ for each thickness is determined for each bias potential. Examples of these results are shown in ESI-2 in the ESI.† Alternatively, a graphical analysis of Fig. 2 permits direct determination of $R = 1/G$ as the diameter semicircle, whereas the frequency of the maximum value of the semicircle corresponds to $k$ and finally $C_\mu = G/k$.

Fig. 3 demonstrates how a mesoscopic approach compares with standard DC analysis§ for molecular junctions based on azobenzene for seven different thicknesses (refer to ESI-2†). Fig. 3(a) shows the modulus of the logarithm of DC electric density current (lines) *versus* bias voltage compared with those results obtained by IS measurements (symbols); Fig. 3(b) and (c) show the logarithm of conductance and logarithm of $k$ *versus* bias as obtained by IS. It is well-known that in azobenzene

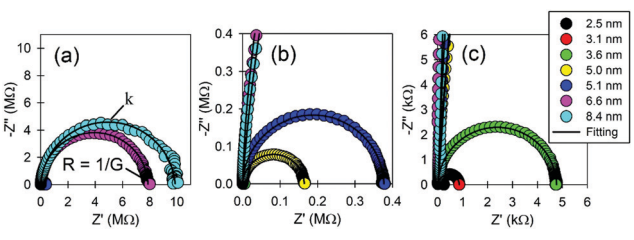


Fig. 2 (a) Impedance measurements (Nyquist diagrams) and the variation of the impedance pattern as a function of the thickness (at 0 bias), demonstrating, as expected, a higher impedance response as a function of the thickness. (b) and (c) Corresponds to the magnification of (a). Typically, these Nyquist diagrams demonstrates the presence of a single $1/k$ time constant.

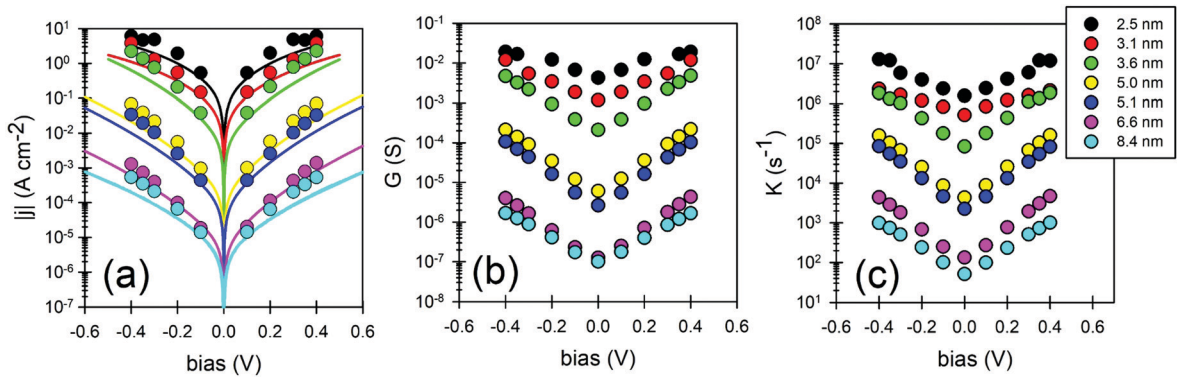


Fig. 3 (a) Logarithm of the modulus of current *versus* bias voltage for seven different thicknesses (lines are DC and symbols are AC measurements). (b) Corresponds to $G$ and (c) $k$ (both as obtained from AC measurements) as functions of bias for the different thicknesses.

junctions with $L \sim 5$ nm the dominant mechanism is tunneling.[36] Therefore, the linearity observed in $k$ *versus* bias is easily interpreted using $G \propto e^{-\beta L}$ and a logarithm of $k$ is expected to be linearly dependent on $-\beta L$. As shown in Fig. ESI.3 (ESI†), the agreement between $\ln(j)$ at $V = 0.1$ V determined from IS results and from DC current–voltage curves is excellent ($r^2 = 99.8\%$) across the seven thicknesses studied.

Additionally, since $j = GV$, we can use the $G(V)$ obtained from IS spectra in Fig. 3(b) to reproduce $j$ over a larger bias range as shown in Fig. 4(b) and (d) (please refer to ESI-2† for examples) then compared to the experimental DC curves in Fig. 4(a) and (c). The agreement between IS-predicted and experimental $I$–$V$ curves is within a factor of 4 over $>3$ orders of magnitude of the current. For instance, an appropriate correlation is illustrated for current densities obtained in both DC and AC methods ($r^2 = 99.8\%$, Fig. ESI.3†). Also, the natural logarithm dependence of the current signal *versus* thickness $L$, as given by the attenuation plot $\ln|j| \propto -\beta L$, is in agreement with previous work (*i.e.* $\beta = \sim 2.6$ nm$^{-1}$)[37] using both methodologies (see Fig. ESI.4†). The remaining differences can be explained by an additional displacement current contribution $i_d$ (arising from the intrinsic dynamics associated with[38] mesoscopic phenomena) in the IS mode of measurement, *i.e.* $i_d \propto \varepsilon(dV/dt)$, where $\varepsilon$ is the dielectric constant and $dV/dt$ is the voltage perturbation with time. Furthermore, the IS technique considers a wide range of frequencies for $G$, whereas the DC measurement is made with a single scan rate (100 mV s$^{-1}$). While there are differences between the two techniques, as can be seen in Fig. 3(a) (symbols and lines), the similarity of $j$–$V$ shape and thickness dependence is apparent in Fig. 4 and indicates that both methods are governed by similar physical principles.

Given that injection into molecular orbitals in a molecular junction has similar physics and chemistry to redox exchange between an electrode and a tethered redox center, the correspondence between IS and DC scanning results is reasonable. For example, the exponential behavior of $k$ on bias in both molecular junctions [Fig. 3(c)] and redox monolayers[1,11] is an indication that both involve similar bias-dependent kinetics.[39–41] Although IS methods have been used previously to characterize molecular junctions,[36,42,43] the addition of mesoscopic principles

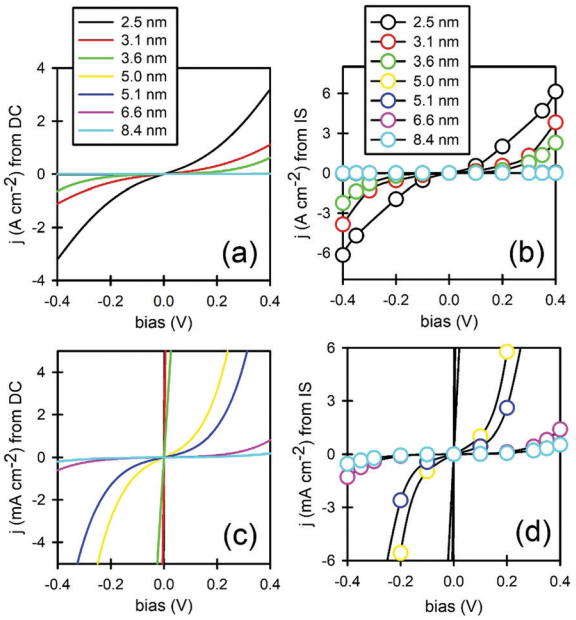


Fig. 4 Equivalence between $J$–$V$ curves obtained from DC (a) and (c) and IS (b) and (d) curves for seven different thickness as measured in azobenzene molecular junctions. IS-obtained curves were constructed through the definition of $G$ discussed in the text and by knowing that $j = GV$. (c) and (d) are enlarged views of the low current regions of (a) and (b), respectively.

significantly expands the physical insights available. Mesoscopic resistive and capacitive terms measurable by IS ultimately control the behavior of both molecular junctions and redox active monolayers, although $C_\mu$ and $G$ are always interdependent. Electrochemical charge transfer generally involves mobile ions, solvent, and double layer formation, but these are additions to the basic charge transfer event present in both electrochemistry and electronics. Furthermore, injection in molecular junctions may also involve thermionic emission[44] and/or field ionization[45] which are unlikely in conventional electrochemical applications.

In conclusion, the rate of electron transfer between an electrode and a redox active monolayer is related to the injection rate observed in molecular electronics, and both are dependent on $k$, $C_\mu$ and $G$. $k$ follows exponential behavior as a function of applied

 

bias which controls the non-linear behavior between current and voltage observed in both electrochemistry and molecular junctions.

## Conflicts of interest

There are no conflicts to declare.

## Acknowledgements

Dr Adriano Santos acknowledges CAPES (88887.463447/2019-00) for his Scholarship and Professor Bueno acknowledges FAPESP for the financial support. Professor Bueno also acknowledges CNPq for an individual support due to his head of research activities in São Paulo State University. Prof. McCreery and Dr Tefashe acknowledge support from Alberta Innovates. Prof. Bueno acknowledges the support of FAPESP for the financial support (2017/24839-0) and CNPq.

## Notes and references

‡ Impedance spectroscopy (IS) was carried out using an AUTOLAB potentiostat equipped with a frequency response analysis (FRA) module and NOVA software from Metrohm. Conditions: frequency range from 5 MHz to 0.1 Hz (~170 frequencies logarithmically arranged), amplitude of 10 mV. Bias potentials of 0 V, ±100 mV, ±200 mV, ±300 mV, ±350 mV, ±400 mV.

§ *I–V* curves were obtained using an AUTOLAB potentiostat controlled by Nova software from Metrohm. Conditions: bias potentials ranging from −0.4 V to 0.4 V, at 100 mV $s^{-1}$.

1 P. R. Bueno, *The Nanoscale Electrochemistry of Molecular Contacts*, Springer, 2018.
2 R. Venkatramani, E. Wierzbinski, D. H. Waldeck and D. N. Beratan, *Faraday Discuss.*, 2014, **174**, 57–78.
3 L. Xiang, J. L. Palma, Y. Li, V. Mujica, M. A. Ratner and N. Tao, *Nat. Commun.*, 2017, **8**, 14471, DOI: 10.1038/ncomms14471.
4 F. R. F. Fan, J. P. Yang, L. T. Cai, D. W. Price, S. M. Dirk, D. V. Kosynkin, Y. X. Yao, A. M. Rawlett, J. M. Tour and A. J. Bard, *J. Am. Chem. Soc.*, 2002, **124**, 5550–5560.
5 R. P. Andres, J. D. Bielefeld, J. I. Henderson, D. B. Janes, V. R. Kolagunta, C. P. Kubiak, W. J. Mahoney and R. G. Osifchin, *Science*, 1996, **273**, 1690–1693.
6 Z. J. Donhauser, B. A. Mantooth, K. F. Kelly, L. A. Bumm, J. D. Monnell, J. J. Stapleton, D. W. Price, A. M. Rawlett, D. L. Allara, J. M. Tour and P. S. Weiss, *Science*, 2001, **292**, 2303–2307.
7 C. Joachim, J. K. Gimzewski and A. Aviram, *Nature*, 2000, **408**, 541–548.
8 A. Nitzan and M. A. Ratner, *Science*, 2003, **300**, 1384–1389.
9 D. Porath, A. Bezryadin, S. de Vries and C. Dekker, *Nature*, 2000, **403**, 635–638.
10 M. A. Reed, C. Zhou, C. J. Muller, T. P. Burgin and J. M. Tour, *Science*, 1997, **278**, 252–254.
11 P. R. Bueno, *Anal. Chem.*, 2018, **90**, 7095–7106.
12 M. Hromadova and F. Vavrek, *Curr. Opin. Electrochem.*, 2020, **19**, 63–70.
13 M. Kilgour and D. Segal, *J. Chem. Phys.*, 2015, **143**, 024111, DOI: 10.1063/1.4926395.
14 S. Valianti and S. S. Skourtis, *J. Phys. Chem. B*, 2019, **123**, 9641–9653.
15 R. L. McCreery, *Chem. Rec.*, 2012, **12**, 149–163.
16 P. R. Bueno, T. A. Benites and J. J. Davis, *Sci. Rep.*, 2016, **6**, 18400.
17 Y. A. Berlin and M. A. Ratner, *Radiat. Phys. Chem.*, 2005, **74**, 124–131.
18 X. S. Zhou, L. Liu, P. Fortgang, A. S. Lefevre, A. Serra-Muns, N. Raouafi, C. Amatore, B. W. Mao, E. Maisonhaute and B. Schollhorn, *J. Am. Chem. Soc.*, 2011, **133**, 7509–7516.
19 S. H. Choi, C. Risko, M. C. R. Delgado, B. Kim, J.-L. Bredas and C. D. Frisbie, *J. Am. Chem. Soc.*, 2010, **132**, 4358–4368.
20 M. Baghbanzadeh, P. F. Pieters, L. Yuan, D. Collison and G. M. Whitesides, *ACS Nano*, 2018, **12**, 10221–10230.
21 S. Chang, J. He, P. Zhang, B. Gyarfas and S. Lindsay, *J. Am. Chem. Soc.*, 2011, **133**, 14267–14269.
22 C. E. Smith, S. O. Odoh, S. Ghosh, L. Gagliardi, C. J. Cramer and C. D. Frisbie, *J. Am. Chem. Soc.*, 2015, **137**, 15732–15741.
23 L. Yuan, L. Wang, A. R. Garrigues, L. Jiang, H. V. Annadata, M. Anguera Antonana, E. Barco and C. A. Nijhuis, *Nat. Nanotechnol.*, 2018, **13**, 322–329.
24 F. C. Simeone, H. J. Yoon, M. M. Thuo, J. R. Barber, B. Smith and G. M. Whitesides, *J. Am. Chem. Soc.*, 2013, **135**, 18131–18144.
25 U. M. Tefashe, C. Van Dyck, S. K. Saxena, J.-C. Lacroix and R. L. McCreery, *J. Phys. Chem. C*, 2019, **123**, 29162–29172.
26 J. A. Fereiro, G. Porat, T. Bendikov, I. Pecht, M. Sheves and D. Cahen, *J. Am. Chem. Soc.*, 2018, **140**, 13317–13326.
27 Y. Zang, S. Ray, E. D. Fung, A. Borges, M. H. Garner, M. L. Steigerwald, G. C. Solomon, S. Patil and L. Venkataraman, *J. Am. Chem. Soc.*, 2018, **140**, 13167–13170.
28 E. D. Fung, D. Gelbwaser, J. Taylor, J. Low, J. Xia, F. Jradi, I. Davydenko, L. M. Campos, S. Marder, U. Peskin and L. Venkataraman, *Nano Lett.*, 2019, **19**, 2114–2120.
29 E. Wierzbinski, R. Venkatramani, K. L. Davis, S. Bezer, J. Kong, Y. Xing, E. Borguet, C. Achim, D. N. Beratan and D. H. Waldeck, *ACS Nano*, 2013, **7**, 5391–5401.
30 A. Nitzan, *J. Phys. Chem. A*, 2001, **105**, 2677–2679.
31 P. R. Bueno, F. C. B. Fernandes and J. J. Davis, *Nanoscale*, 2017, **40**, 15362–15370.
32 W. C. Ribeiro, L. M. Goncalves, S. Liebana, M. I. Pividori and P. R. Bueno, *Nanoscale*, 2016, **8**, 8931–8938.
33 F. F. Hudari, G. G. Bessegato, F. C. B. Fernandes, M. V. B. Zanoni and P. R. Bueno, *Anal. Chem.*, 2018, **90**, 7651–7658.
34 F. A. Gutierrez, F. C. B. Fernandes, G. A. Rivas and P. R. Bueno, *Phys. Chem. Chem. Phys.*, 2017, **19**, 6792–6806.
35 A. Morteza Najarian, B. Szeto, U. M. Tefashe and R. L. McCreery, *ACS Nano*, 2016, 8918.
36 A. J. Bergren, R. L. McCreery, S. R. Stoyanov, S. Gusarov and A. Kovalenko, *J. Phys. Chem. C*, 2010, **114**, 15806.
37 S. Y. Sayed, J. A. Fereiro, H. Yan, R. L. McCreery and A. J. Bergren, *Proc. Natl. Acad. Sci. U. S. A.*, 2012, **109**, 11498–11503.
38 J. Gabelli, G. Feve, J. M. Berroir, B. Placais, A. Cavanna, B. Etienne, Y. Jin and D. C. Glattli, *Science*, 2006, **313**, 499–502.
39 K. J. Vetter, *Electrochemical Kinetics: Theoretical and Experimental Aspects*, Academic Press, 1967.
40 A. J. Bard and L. R. Faulkner, *Electrochemical Methods: Fundamentals and Applications*, John Wiley & Sons, New York, 2001.

41 L. Yuan, L. Wang, A. R. Garrigues, L. Jiang, H. V. Annadata, M. Anguera Antonana, E. Barco and C. A. Nijhuis, *Nat. Nanotechnol.*, 2018, **13**, 322.
42 C. S. S. Sangeeth, A. T. Demissie, L. Yuan, T. Wang, C. D. Frisbie and C. A. Nijhuis, *J. Am. Chem. Soc.*, 2016, **138**, 7305.
43 P. Chandra Mondal, U. M. Tefashe and R. L. McCreery, *J. Am. Chem. Soc.*, 2018, **140**, 7239.
44 Z. Karipidou, B. Branchi, M. Sarpasan, N. Knorr, V. Rodin, P. Friederich, T. Neumann, V. Meded, S. Rosselli, G. Nelles, W. Wenzel, M. A. Rampi and F. von Wrochem, *Adv. Mater.*, 2016, **18**, 3473–3480.
45 H. Yan, A. J. Bergren, R. McCreery, M. L. Della Rocca, P. Martin, P. Lafarge and J. C. Lacroix, *Proc. Natl. Acad. Sci. U. S. A.*, 2013, **14**, 5326–5330.